Rapid, femtomolar bioassays in complex matrices combining microfluidics and magnetoelectronics

S. P. Mulvaney [a], C. L. Cole [a,b], M. D. Kniller [a], M. Malito [a], C. R. Tamanaha [a], J. C. Rife [a], M. W. Stanton [a], L. J. Whitman [a,*]

[a] *Naval Research Laboratory, Washington, DC 20375 USA*

[b] *Current address: National Air and Space Museum, Smithsonian Institution, Washington, DC 20013 USA*

Abstract

A significant challenge for all biosensor systems is to achieve high assay sensitivity and specificity while minimizing sample preparation requirements, operational complexity, and sample-to-answer time. We have achieved multiplexed, unamplified, femtomolar detection of both DNA and proteins in complex matrices (including whole blood, serum, plasma, and milk) in minutes using as few as two reagents by labeling conventional assay schemes with micrometer-scale magnetic beads, and applying fluidic force discrimination (FFD). In FFD assays, analytes captured onto a microarray surface are labeled with microbeads, and a controlled laminar flow is then used to apply microfluidic forces sufficient to preferentially remove only nonspecifically bound bead labels. The density of beads that remain bound is proportional to the analyte concentration and can be determined with either optical counting or magnetoelectronic detection of the magnetic labels. Combining FFD assays with chip-based magnetoelectronic detection enables a simple, potentially handheld, platform capable of both nucleic acid hybridization assays and immunoassays, including orthogonal detection and identification of bacterial and viral pathogens, and therefore suitable for a wide range of biosensing applications.

Keywords: Biosensor; DNA hybridization assay; Fluidic force discrimination; Immunoassay; Magnetic bead; Magnetic detection.

---

* Corresponding author. Tel.: +1 202 404 8845; fax: + 1 202 767 3321.
E-mail address: whitman@nrl.navy.mil (L.J. Whitman)

22 March 2007

Report Documentation Page

Form Approved
OMB No. 0704-0188

1. REPORT DATE	2. REPORT TYPE	3. DATES COVERED
22 MAR 2007		**00-00-2007 to 00-00-2007**

4. TITLE AND SUBTITLE	5a. CONTRACT NUMBER
Rapid, femtomolar bioassays in complex matrices combining microfluidics and magnetoelectronics	5b. GRANT NUMBER
	5c. PROGRAM ELEMENT NUMBER
6. AUTHOR(S)	5d. PROJECT NUMBER
	5e. TASK NUMBER
	5f. WORK UNIT NUMBER
7. PERFORMING ORGANIZATION NAME(S) AND ADDRESS(ES) **Naval Research Laboratory,4555 Overlook Avenue SW,Washington,DC,20375**	8. PERFORMING ORGANIZATION REPORT NUMBER
9. SPONSORING/MONITORING AGENCY NAME(S) AND ADDRESS(ES)	10. SPONSOR/MONITOR'S ACRONYM(S)
	11. SPONSOR/MONITOR'S REPORT NUMBER(S)

12. DISTRIBUTION/AVAILABILITY STATEMENT
Approved for public release; distribution unlimited

13. SUPPLEMENTARY NOTES
Biosensors and Bioelectronics, Volume 23, Issue 2, 30 September 2007, Pages 191-200

14. ABSTRACT

A significant challenge for all biosensor systems is to achieve high assay sensitivity and specificity while minimizing sample preparation requirements, operational complexity, and sample-to-answer time. We have achieved multiplexed, unamplified, femtomolar detection of both DNA and proteins in complex matrices (including whole blood, serum, plasma, and milk) in minutes using as few as two reagents by labeling conventional assay schemes with micrometerscale magnetic beads, and applying fluidic force discrimination (FFD). In FFD assays, analytes captured onto a microarray surface are labeled with microbeads, and a controlled laminar flow is then used to apply microfluidic forces sufficient to preferentially remove only nonspecifically bound bead labels. The density of beads that remain bound is proportional to the analyte concentration and can be determined with either optical counting or magnetoelectronic detection of the magnetic labels. Combining FFD assays with chip-based magnetoelectronic detection enables a simple, potentially handheld, platform capable of both nucleic acid hybridization assays and immunoassays, including orthogonal detection and identification of bacterial and viral pathogens, and therefore suitable for a wide range of biosensing applications.

15. SUBJECT TERMS

16. SECURITY CLASSIFICATION OF:			17. LIMITATION OF ABSTRACT	18. NUMBER OF PAGES	19a. NAME OF RESPONSIBLE PERSON
a. REPORT **unclassified**	b. ABSTRACT **unclassified**	c. THIS PAGE **unclassified**	**Same as Report (SAR)**	**31**	

1. Introduction

Rapid advancements in biosensor technology over the past several decades has led to widespread implementation across a variety of application fields, ranging from biodefense (Hindson et al., 2005; Ivnitski et al., 2003; Lim et al., 2005; Peruski and Peruski, 2003), to medical diagnostics (Andreotti et al., 2003; Gao et al., 2004), to environmental monitoring (Baeumner, 2003; Farre and Barcelo, 2003). The diversity of applications and sample matrices results in a nonuniform set of operational requirements. Even if one only considers biodefense applications, the paradigms of detect-to-protect, detect-to-treat, and detect-to-monitor place different emphases on sensitivity, selectivity, portability, and sample-to-answer time. Meanwhile, there is an emerging need for a decentralized laboratory with simple, portable systems suitable for use by non-technical personnel, such as first-responders, infantry, and point-of-care medical staff. Within this vast operational landscape, it is unlikely that a single technology will satisfy all applications; therefore, specific end-user requirements will guide the selection among promising approaches.

The most promising biosensor technologies distinguish themselves across several operational characteristics, including but not limited to sensitivity, selectivity, sample-to-answer time, portability, operational complexity, and cost. For example, the bio-bar-code assay of Mirkin and co-workers has state-of-the-art analytical sensitivity and selectivity for the detection of nonamplified nucleic acids and proteins (Nam et al., 2004; Stoeva et al., 2006). Using this technology, attomolar target concentrations can be detected, without the complications of amplification (e.g. via polymerase chain reaction (PCR)), because the bar-code DNA provides signal amplification. In a competing approach, Lieber and co-workers have achieved highly sensitive, multiplexed, label-free detection of cancer markers in complex matrices using an

elaborate nanowire-based device (Zheng et al., 2005). They report detection of prostate specific antigen in undiluted (but de-salted) serum at concentrations as low as 0.9 pg/ml. In contrast, extremely rapid (<5 min) and simple lateral flow immunoassay kits are available from a number of sources, but these kits perform poorly for pathogen detection and are not easily multiplexed (Lim et al., 2005).

The majority of biosensors incorporate solid-phase binding assays whereby target analytes are captured by biomolecular recognition and labeled with "reporters," such as fluorophores, enzymes, radiolabels, nanoparticles, or electrochemically active species. In general, the means for detecting the reporter label is independent of the target capture and labeling assay. System performance (i.e. sensitivity, specificity, reproducibility) is rarely limited by the ability to detect the labels, but rather by the background signal associated with nonspecific adsorption in the assay. A classic example is nucleic assay hybridization microarrays (gene chips) incorporating fluorescence labeling and detection (Epstein et al., 2002; Michalet et al., 2003). Typically, the target oligonucleotides are fluorescently labeled during PCR amplification, and multiple surfactant-laden wash steps and/or temperature cycles are applied to remediate nonspecific binding to noncomplementary capture probe spots. However, the performance of microarrays is not usually limited by the ability to detect the fluorescence. A similar state of affairs exists for conventional enzyme-linked immunosorbent assays (ELISAs) and related solid-phase immunoassays, where performance is typically limited by the background label density, not label detection.

The ubiquity of reporter label-based bioassays arises from the wide choice of labels that can be applied to common assay schemes. Labels used in bioassays are generally molecular or nanoscale in size in order to match the size of the biomolecular recognition probes and analyte

targets. In contrast, micrometer-scale labels — such as microbeads used for magnetic separation and as assay substrates — have been discounted as labels based on concerns about their large relative size (Graham et al., 2004; Wang et al., 2005). However, we find microbead labels offer two significant advantages over smaller labels that far outweigh any disadvantages from the size mismatch. First, it is far simpler to detect low numbers of microbeads than molecular fluorophores, chromophores, or nanoparticles, with individual microbeads readily counted with routine optical microscopy (Lee et al., 2000; Mulvaney et al., 2004) or magnetic detection (Rife et al., 2003; Rife and Whitman, 2004). Second, and more significantly, we find that if a controlled laminar flow is maintained at the capture surface, fluidic drag forces can be applied to the microbead labels to preferentially remove nonspecifically bound labels and thereby dramatically improve the assay performance (Rife and Whitman, 2004). We have leveraged these advantages and use magnetic microbeads to label nucleic acid hybridization assays and protein immunoassays performed on top of a microarray of magnetoelectronic sensors. This combination of microfluidics and magnetoelectronics enables highly sensitive and specific multiplexed detection in minutes in complex sample matrices.

2. Materials and methods

2.1. Assay fluidics

Two flow cells were used for this work. The data from Fig. 1 was collected in straight channels 2 cm long × 250 μm high × 800 μm wide with all capture spots located in the center of a channel. All other assays were performed in an acrylic assembly incorporating multiple flow cells mounted on a microscope slide (see Supplementary Fig. 1 online). Each flow cell had central dimensions of 2.8 mm long × 2.2 mm wide × 100 μm high, with tapered entrance and exits to assure uniform, laminar flow of reagents across the capture spots, as discussed in detail in a previous publication (Tamanaha et al., 2002). In particular, the flow cell design creates a very uniform fluid velocity across the middle of the channel where the assay occurs, ensuring consistent spot-to-spot application of fluidic forces. Note that the geometry of this cell produces drag forces on the microbeads approximately twice as large as in the straight channels at identical flow rates. The flow rates were controlled with a peristaltic pump (Instech Laboratories, Inc.).

2.2. Substrate Surface Chemistry

Standard microscope slides coated with silicon nitride were purchased from Lance Goddard Films. As-received slides were dipped in 1% HF solution, rinsed with copious amounts of H_2O, and dried in a N_2 stream. They were then immediately plasma cleaned in ~70% humidified air for 50 min. at 135W, producing a combination of hydroxyl and primary amine groups (Stine et al., 2007). The primary amines were reacted with a 20% aqueous glutaraldehyde (Sigma-Aldrich) solution for 2 hours. The excess glutaraldehyde was aspirated and the slide reacted with

1.25 mg/ml NeutrAvidin (Pierce Biotechnology, Inc.) for 45 min. Finally, coated slides were rinsed with H_2O, dried in a N_2 stream, and stored at 4 °C until used.

2.3. Microbead labels

Two types of commercially available beads were used in this work. Both work off of the Dynal M-280 bead (Invitrogen) and are conjugated with either sheep anti-rabbit antibodies or oligo$(dT)_{25}$ probes.

2.4. DNA Hybridization Assays

All DNA was purchased from Oligos Etc. Inc. Biotinylated capture oligonucleotides were immobilized on a NeutrAvidin-coated slide by spotting with Rapidograph pens as previously reported(Sheehan et al., 2003). The ssDNA target was prehybridized with the label probes in solution for at least 15 min. The capture and label probes were complementary to adjacent regions of the ssDNA target. The target-label complex was flowed at room temperature through the flow cell over the slide at 10 μL/min for 15 min unless otherwise noted. Dynal M-280 oligo$(dT)_{25}$ beads were then introduced and allowed to settle for 3 min. FFD was performed with a 5x SSC buffer at ~33 μL/min for 3–5 min. (Force discrimination was completed in <1 min, but additional time was required to flush all beads from the tubing.)

2.5. DNA capture probe sequences

Complementary: 5’-CGATGCTGTGGCTCGATATAA-biotin-3’

Positive control: 5’-AAAAAAAAAAAAAAAAAAAAAA-biotin-3’

Noncomplementary: 5’-TACTTAGTAATTGGGAAGCTTGTA-biotin-3’

2.6. DNA target sequence

5’-TTATATCGAGCCACAGCATCGTGATGTTTTACAAACGAACAAGAAATAAAT CTA-3’

2.7. DNA label probe sequence

5’-AAAAAAAAAAAAAAAAAAAAAAAAAAAAAATAGATTTATTTCTTGTTCGTTT GTAAA-3’

2.8. Blood Sample Preparation

Beagle donors were bled for whole blood, plasma, and serum by Innovative Research, Inc. The plasma samples were filtered with a 0.45 μm syringe filter (Fisher Scientific) to remove cellular debris, but otherwise used as received. Whole blood was used as received.

2.9. Immunoassays

Materials for multiplexed detection of ricin A chain (RCA) and staphyloccal enterotoxin B (SEB) were obtained from government sources. Either 218 pM (7 ng/ml) RCA or 35 pM (1 ng/ml) SEB was spiked into PBS buffer. Biotinylated goat anti-ricin and biotinylated sheep anti-SEB antibodies were spotted onto a functionalized slide. The sample containing the target toxin was introduced into the flow cell and incubated at room temperature without flow for 5 min. Then rabbit anti-RCA or rabbit anti-SEB was incubated without flow for 5 min. Dynal M-280 sheep anti-rabbit beads were then introduced and allowed to settle for 3 min. FFD was performed with PBS buffer as described above. The remaining concentrations for the RCA dose-response curve were run in like manner.

For IgG targets, biotinylated whole IgG antibodies from mouse and canine (Rockland Immunochemicals) were spotted onto a slide. The rabbit anti-mouse IgG target (Pierce) was spiked into plasma at 13 fM (2 pg/ml), or spiked into blood at 130 fM which was then diluted 10:1 in PBS buffer. The sample containing the target protein was introduced into the flow cell and incubated at room temperature without flow for 5 min. Dynal M-280 sheep anti-rabbit beads were then introduced and allowed to settle for 3 min. FFD was performed with PBS buffer as described above.

Troponin I (Fitzgerald Industries International, Inc.) was spiked into canine blood serum at 280 fM (10 pg/ml). Biotinylated goat anti-troponin I antibodies (Fitzgerald) were spotted onto a slide and exposed to the sample for 5 min as above. A "double" indirect immunoassay was performed, with mouse anti-troponin I (Fitzgerald) antibodies introduced into the cell and incubated for 5 min, followed by rabbit anti-mouse IgG antibodies, also incubated for 5 min. The assay was completed as above using sheep anti-rabbit beads. (This unusual "double" indirect scheme was employed to make economical use of existing stocks of immunobeads and antibodies.)

RCA toxoid was spiked into whole milk at 630 fM (20 pg/ml). Biotinylated goat anti-ricin antibodies were spotted onto a slide and exposed to the sample for 5 min as above. Then a simple indirect immunoassay was performed, with rabbit anti-ricin antibodies (5 min), and sheep anti-rabbit beads as above.

2.10. Combined Immunoassay and DNA Hybridization Assay

Capture probes were immobilized on the slide as described above. The sample consisted of PBS buffer spiked with 6.5 nM rabbit anti-canine IgG and 5 nM ssDNA prehybridized with the label probe. The sample was flowed at room temperature through the cell at 10 μL/min for 15

min. The bead solution, consisting of 70% oligo$(dT)_{25}$ beads and 30% sheep anti-rabbit beads, was introduced as above followed by FFD with PBS buffer.

2.11. On-Chip RCA Assay

A Bead ARray Counter (BARC®) chip was functionalized with NeutrAvidin as described above. The functionalized chip was spotted with biotinylated antibodies specific for RCA and SEB as shown in Fig. 6b. The spotted chip was sealed in a microfluidics cartridge with the same tapered flow cell design as described above (Fig. 6a). RCA toxoid was spiked into serum at 318 fM (10 ng/ml) and incubated without flow for 5 min. Then a simple indirect immunoassay was performed, with rabbit anti-ricin antibodies (5 min), and sheep anti-rabbit beads as described above. The chip was similar in design to that described previously (Rife et al., 2003), but was fabricated with more sensitive GMR sensors (providing a 30-times larger signal per bead).

2.12. Bead Counting

The density of beads remaining after FFD is proportional to the analyte concentration, and can be determined with either optical counting or magnetoelectronic detection. For optical counting, an image of the capture spot is collected utilizing a CCD camera and optical microscope. Our custom LabVIEW-based application then defines a 200 μm-diameter circle in the center of the capture spot. Using National Instrument Vision software, the number of beads within that circle is determined by setting a binary threshold in the bright field image to delineate the beads, calculating the area covered by beads, and then dividing by the average area of a single bead. Analyzing the images in this manner allows for accurate bead counts even when some beads are too close (or touching) for the software to resolve them individually. The total image analysis time is currently <2 min per spot, dominated by the time required to manually

locate and focus on each capture spot. With automated image capture, under development, we expect the total image analysis time to be <30 s per spot.

Magnetoelectronic bead counting is accomplished on a BARC® chip as described previously (Rife et al., 2003). All beads captured above a GMR sensor contribute to the measured resistance with a linear response from ~1 to 1000 Dynabeads. The current total read time for a BARC®-III chip with 64 sensors is ~2 min, with the limiting factor being data transmission across a serial cable. We are in the process of converting to a USB interface that will reduce the total read time to <5 s.

3. Results

Atomic force microscopy studies have demonstrated that the binding strengths of specific biological ligand-receptor interactions are at least an order of magnitude greater than those of the ligand nonspecifically interacting with receptors or nonfouling surfaces (Lee et al., 1994; Metzger et al., 1999). Several bioassay methods have been developed that exploit this differential in binding by applying magnetic forces to microparticle labels, a technique known as magnetic force discrimination (MFD) (Baselt et al., 1998; Edelstein et al., 2000; Lee et al., 2000; Rife et al., 2003). With commercially available paramagnetic microbeads and simple magnetic geometries, MFD forces are limited to ~1 pN; therefore, the nonfouling properties of the substrate must be very tightly controlled for MFD to be effective. In contrast, under easily achieved laminar flow in microfluidic channels, fluidic forces on microparticles can exceed 100 pN (Chang and Hammer, 1996), making fluidic force discrimination (FFD) effective in a much wider range of assay implementations.

The basic schemes along with the biophysics of FFD assays are demonstrated in Fig. 1**,** as applied to conventional solid-phase binding assays performed on NeutrAvidin-functionalized

substrates (Narang et al., 1997). For hybridization assays, we use biotinylated, single-stranded DNA (ssDNA) capture probes; secondary label probes that are complementary to an adjacent nucleotide sequence on the target and terminated with an oligo$(dA)_{25}$ tail; and oligo$(dT)_{25}$-functionalized microbead labels. In this scheme, ssDNA targets can be detected *without further modification*. For immunoassays, the immunochemical complex sandwiches the analyte between two antibody probes: a biotinylated capture antibody and a microbead-immobilized antibody active against a second epitope on the analyte. Alternately, indirect immunoassays can be performed by using secondary label antibodies and immunobeads active against the Fc fragment of the label (advantageous for multiplexed assays using a single type of immunobead). For all assay schemes, following the capture of the targeted analyte(s) (and secondary labeling, if required), the capture surface is exposed to a high density of microbeads, thereby labeling those locations where target analytes are bound to the surface. We then briefly introduce a controlled laminar flow of buffer across the surface, applying a drag force on each bead that is less than the rupture strength of a specific DNA duplex (ca. 800–1200 pN) (Lee et al., 1994) or immunochemical complex (ca. 60–250 pN) (Kaur et al., 2004), but greater than that required to remove beads bound to the surface by weak, nonspecific interactions (ca. 0.1–10 pN). *Note that simple wash steps cannot achieve effective FFD, because non-uniform and/or turbulent flows induce a wide range of uncontrolled forces, leading to random and indiscriminant label removal.*

In principle, the composition (i.e. pH, stringency, salt) and temperature of the buffer used for the FFD step could be used to modulate the strength of both specific and nonspecific biomolecular interactions along with the balance between those interactions and the fluidic force applied. For example, by increasing the stringency and temperature, FFD has the potential to selectively remove near-target nucleotides having one or more base-pair mismatches with a

capture probe, and therefore identify single nucleotide polymorphisms (SNPs). This potentially exciting application of FFD assays will be the subject of future investigation.

The force applied to a microbead during FFD is a function of the volumetric flow, channel geometry, buffer viscosity, and bead diameter (Rife and Whitman, 2004). Using the model of Chang and Hammer (Fig. 1b) (Chang and Hammer, 1996), the applied forces can be estimated from the viscous Stokes force and torque (Goldman et al., 1967). For a bead tethered to a surface by molecular interactions, the tension force on the tether is much larger than the simple Stokes force, because the offset between the bead-surface contact point and the bead-tether contact point creates a mechanical lever. For example, with a 1.4 μm-radius bead attached by a 10 nm-long tether in a flow cell 250 μm high × 800 μm wide, a flow rate of 33 μL/min produces a tension force ~100 pN. Although the flow rate needed to remove a microbead depends on a number of variables, the wide range of forces accessible with microscale beads and reasonable microfluidic flow rates (up to 100 μL/min) makes it straightforward in practice to determine an effective rate and duration for FFD. Note that because the laminar flow velocity is zero at the surface, the force decreases rapidly with bead radius (as $a^{5/2}$), such that a 100 nm-radius bead under these conditions experiences a tension force <<0.1 pN. *Therefore, FFD is not possible with nanoparticle labels for any practical microfluidic flow rates.*

An implementation of FFD for multiplexed ssDNA detection is demonstrated in the optical micrographs shown in Fig. 1c. In this assay, three different capture probes were immobilized on the substrate, as follows: a positive control spot for microbead binding (biotinylated oligo$(dA)_{25}$); a capture probe complementary to the target sequence (two spots); and a capture probe complementary to a second nucleotide sequence (two spots). The left micrographs (0 μL/min) show the surface after hybridization with the target (10 nM) and the introduction of

microbead labels. The right micrographs show the surface following FFD (33 μL/min), where the specific label density is more than 100 times greater than the nonspecific background. Notably, the background on the capture probe spots that are not complementary to the target is indistinguishable to that on the surrounding NeutrAvidin substrate (chosen specifically for its nonfouling properties). As the flow rate (and force) is further increased, specifically bound beads are eventually removed (see Supplemental Fig. 2 online), demonstrating the effectiveness of laminar fluidic forces for fully controlling microbead-labeled binding assays.

Because individual microbead labels are easily detected, and force discrimination dramatically reduces the background label density, the sensitivity of FFD assays is limited only by diffusive transport and biomolecular binding affinities. Fig. 2a demonstrates the detection of a 10 fM concentration of a 54-nt long ssDNA sample. Excellent specificity is achieved with only 30 min of hybridization at room temperature and 300 μL of sample (flowed at 10 μL/min). Under these diffusion-limited conditions, each 200 μm-diameter capture spot will interact with at most 7000 target molecules (Sheehan and Whitman, 2005). Statistically, each of the ~300 specifically bound microbeads labels a *single* captured target. The overall hybridization and labeling efficiency was 4%, suggesting that with more optimal hybridization conditions the sensitivity could potentially be improved by at least an order of magnitude within the same assay time. We observe an approximately logarithmic dose-response from femtomolar to micromolar DNA target concentrations—a dynamic range of nine orders of magnitude (Fig. 2b). A statistically relevant error analysis is still incomplete, but our preliminary data indicates reproducibility greater than 85% (which we expect to improve with automation).

A significant advantage of FFD assays is that the forces applied to the microbead labels are not only applicable for hybridization assays, but can be easily modulated to achieve highly

sensitive and selective immunoassays. In Fig. 3a we demonstrate the multiplexed detection of two protein toxins, ricin A chain (RCA) and staphylococcal enterotoxin B (SEB), using an indirect immunoassay scheme (immobilized capture antibodies, labeling antibodies, and immunobeads specific to the Fc portion of the label antibody). The micrographs clearly demonstrate the even in the presence of a relatively high concentration of either RCA (218 pM, or 7 ng/ml) or SEB toxin (35 pM, or 1 ng/ml), the cross-reactive bead binding after FFD is very low. This discrimination against false positive results is a distinguishing feature of the FFD assay. Similar to the hybridization assay, a dose-response curve was collected for the RCA toxin (Fig. 3b). Again, an approximately logarithmic dose-response was seen over 6 orders of magnitude (pg/ml to μg/ml) with better than 88% reproducibility. For toxins of this size (~ 30 kD), the limit of detection at the time of these assays was in the femtomolar range (~10 pg/ml = ~300 fM).

Beyond facilitating detection and enabling FFD, we believe the relatively large size of the beads contributes to the remarkable sensitivity of the assays. Immunoassays are often limited by the natural process of ligand-receptor association-disassociation as measured as a binding rate constant. These binding constants notably come into play during rinse steps that expose the ligand-receptor complex to buffer (where the analyte ligand concentration is zero), leading to dissociation and loss of previously bound analyte. The immunological complexes in our method are only exposed to buffer for a minute or so before bead binding. After bead introduction, the large relative size of the beads confines a very small volume within the contact area, effectively creating a very high local concentration of analyte and antibodies. The overall effect will be to greatly increase the effective binding constant by inhibiting loss of captured analyte confined under a bead, even when the flow cell is filled with buffer.

We also hypothesize that the extremely large size of the beads compared with the molecular elements contributes to the log-linear shape of our dose response curve and the surprising dynamic range. At low target concentrations, the average spacing between captured target species is greater than the bead diameters, so each bead on average labels a single captured target and each bead can be easily counted. As the captured target concentration increases, the labeling efficiency should increase rapidly at low concentrations, increasing the slope of the response curve. However, at high target concentrations, when the average spacing between captured species becomes less than a bead diameter, steric hindrance and electrostatic repulsion between beads will reduce the labeling efficiency, and thereby suppress the rise of the response. The large dynamic range does, however, come as a tradeoff with analytical resolution; i.e. under our current protocol it would be difficult to distinguish changes in concentration <10x. The unusual biophysics of FFD assays with microbead labels is the subject of an ongoing investigation.

Note that 2.8 μm-diameter beads are not necessarily optimal for FFD assays, but were selected because they are commercially available with appropriate bioconjugation and easily detected by our magnetoelectronic sensors. Smaller microbeads are expected to increase the labeling efficiency and alter the shape of the dose response curve, and may help to increase the fidelity when measuring high target concentrations. However, higher flow rates will be required for FFD, increasing the reagent requirements, and the smaller bead size will require larger volume magnetization per bead and/or an increase in the sensitivity of the magnetoelectronic sensors.

An important aspect of FFD assays is that the force discrimination step occurs in buffer after the binding assay has been completed; therefore, FFD can be applied to any assay scheme that can be labeled with a microbead, such as an ELISA-like immunoassay. In Fig. 4 we demonstrate

multiplexed assays for three different protein targets spiked into various complex matrices with no, or minimal (coarse filtering), sample pretreatment. Target/matrix combinations are included that are pertinent to clinical diagnostics (IgG in plasma, troponin I in serum, Figs. 4a-b) and biodefense (ricin in whole milk, Fig. 4c). All the proteins can be detected at femtomolar concentrations with excellent specificity (specific/nonspecific label density > 10) after simply incubating the sample on the multiplexed capture surface for 5 min (<15 min total assay time).

Perhaps the most challenging bioassay matrix is whole blood, which contains an abundance of proteins, lipids, and cellular material. FFD assays can be performed with high sensitivity and specificity *in whole blood* if simply diluted 10-fold in PBS buffer, as shown in Fig. 4d. This result corresponds to specific protein detection at 130 fM in whole blood with no sample preparation, only two reagents (immunobeads and buffer), and a total assay time of ~10 min. Development of dose response curves for each target in each of the clinical matrices is underway.

The only requirement for a successful FFD assay is that molecular recognition occurs between the targets and specific capture probes and labels. This simplicity is demonstrated by simultaneous DNA and protein detection on a multiplexed microarray *combining* nucleic acid hybridization and immunological recognition (Fig. 5). In this assay, a buffer sample spiked with *both* ssDNA and rabbit anti-canine IgG was exposed to a microarray with six distinct capture spots. At the top and bottom of the flow cell, canine and mouse antibodies were immobilized as the specific and nonspecific immunoassay capture spots, respectively. Across the middle of the flow cell were ssDNA capture spots for a positive control (as above), probes complementary to the DNA target, and a probe for a different DNA target (noncomplementary). Following sample incubation for 15 min, a mixture of oligo$(dT)_{25}$ and anti-rabbit microbead labels was introduced.

After FFD, specific detection of both the DNA and protein targets was achieved. Simultaneous, multiplexed hybridization and immunoassays performed in the same reagent volume is a noteworthy capability(Perrin et al., 2003) and distinguishing characteristic of FFD assays; it demonstrates the approach's potential for orthogonal detection and identification of viruses and bacteria.

One of the advantages FFD offers for biosensing is that microbead labels can be easily resolved with optical microscopy and captured bead densities measured with off-the-shelf particle-counting protocols. A variety of additional advantages can be realized by performing the assay on a substrate with integrated magnetic sensors for direct label detection. Previously, we have described such a BARC® chip having a 64-element array of giant magnetoresistive (GMR) sensors (Rife et al., 2003), that can be incorporated in a microfluidic cell (Fig. 6a). Briefly, under an externally-applied magnetic field, the resistance of each embedded sensor is proportional to the number of (paramagnetic) magnetic beads captured on the surface above it. The results of an on-chip FFD immunoassay are shown in Fig. 6b-c for the detection of 312 pM RCA in *unprocessed bovine serum*. A 7-fold greater bead density is seen on the RCA capture zone with the negative control (SEB) and background (sensors without capture antibodies) being comparable. (The background on the negative capture antibodies is actually slightly lower than on the NeutrAvidin-only areas.) The correlation between optical bead counts and the magnetic signal is also shown, with an average signal of 1.6 μV/bead obtained with the current prototype instrument and chip design. The signal per bead is based purely on magnetoelectronic phenomenon, so it is independent of the assay method and unaffected by the sample matrix. We have repeatedly verified that an assay performed on a chip is equivalent to one performed in the same flow cell geometry on a similarly-functionalized slide with optical bead counting.

The magnetoelectronic assay was performed using a compact Bead Array Sensor System (*cBASS*®) prototype instrument that combines FFD assays and with BARC® chip bead detection. Currently a field portable system (dimensions: 9" x 7" x 6") *cBASS*® employs a reusable microfluidic cartridge and computerized assay control. The total assay time, including sensor interrogation, can be as short as 10 min depending on the assay protocol used.

4. Discussion

As the diversity of biosensing applications continues to expand, no single technology currently meets all required performance criteria, and relatively few are capable of addressing multiple application areas. The most successful systems aim to achieve high assay sensitivity and specificity while minimizing sample preparation requirements, operational complexity, and sample-to-answer time. The tradeoffs between these operational characteristics will ultimately guide end-user selection.

Assay sensitivity and specificity tend to be the primary metric when comparing biosensor systems. For nucleic acid detection, PCR amplification makes possible the detection of <10 copies per sample (Decaro et al., 2006; Hoffmann et al., 2006; Saiki et al., 1985). However, the use of PCR or other primer-based asymmetric amplification schemes introduces significant complexity to sample preparation requirements, complications with real world sample matrices, and difficulties in multiplexing, all of which limit the ability for use outside a controlled laboratory environment. Including homogenous sample extraction with internal amplification, as performed in the bio-bar-code assay (Nam et al., 2004), is one approach to avoid these complications yet still obtain attomolar sensitivity in a few hours. An unamplified, solid-phase assay such as the FFD assay will be limited by diffusion from achieving similar sensitivities. However, multiplexed FFD assays are much simpler, require fewer reagents, can be performed in

complex matrices, and take only minutes, yet still achieve extraordinary sensitivity (fM) for a microarray-based approach. Furthermore, the simplicity of FFD, especially when combined with magnetoelectronic detection, makes it a potentially useful method to rapidly detect and identify nucleic acid amplicons produced by a bio-bar-code or other enzymatic amplification strategy; the inherent sensitivity of FFD assays greatly reduces the amount of amplification required (both in terms of the number of cycles and total time) and eliminates the need for a complex optical system to quantitate fluorescence.

The number and variety of immunoassay approaches for protein and pathogen detection are staggering. Lateral flow assays are simple, rapid tests that can be run by untrained personnel; however, they perform relatively poorly for pathogen detection and are not readily multiplexed. At the other extreme, the approach of Lieber and co-workers utilizing nanowire-based field effect transistors is capable of label-free, multiplexed, and highly sensitive protein detection (Zheng et al., 2005), but requires complex fabrication methods, significant sample preparation, and each sensor has a unique, matrix-dependent dose-response. In comparison, our approach has comparable limits of detection but can be performed in untreated clinical matrices on a substrate as simple as a microscope slide (with optical bead counting).

A battery-powered, hand-portable *cBASS*® instrument, currently under development, will enable rapid, multiplexed immunoassays or nucleic acid amplicon detection in a variety of field settings and unprocessed sample matrices. When combined with in-cartridge bacterial and viral lysing and/or nucleic acid extraction (using one of the many approaches recently developed (Bange et al., 2005; Crowley and Pizziconi, 2005; Erickson and Li, 2004; Lee and Hsing, 2006; Yi et al., 2006)), a capability for direct, highly sensitive pathogen detection is expected. Finally, the ability to perform equivalent, higher throughput assays using optical bead counting means

that a portable assay can be replicated and confirmed in a laboratory setting, an important capability for both biodefense and medical diagnostic applications. We expect the combination of magnetoelectronic labeling and detection with FFD to be a versatile approach for a wide range of biosensing applications.

5. Conclusions

Utilizing fluidic force discrimination assays, we have demonstrated femtomolar detection of both DNA and proteins in a rapid, multiplexed format using as few as two reagents. Our magnetic, microbead labels provide us with several advantages for biosensing. Because the beads are used as a physical label, the assays can directly detect targets out of complex matrices with minimal (and in some cases no) sample processing; the only requirement is that the matrix not interfere with biomolecular recognition. The range of Stokes forces that can be applied to beads with reasonable microfluidic flow rates is ideally suited for modulating biological binding interactions. Finally, the bead labels are readily counted by either optical microscopy or magnetoelectronic sensors, thereby making these assays applicable to both hand-held, first-responder use and higher-throughput, confirmatory analysis in a laboratory setting.

Acknowledgments

This work was supported in part by a Cooperative Research and Development Agreement with Seahawk Biosystems, Inc. (NCRADA-NRL-04-341). The authors would also like to thank Seahawk and SAE Magnetics (H.K. Ltd) for providing the BARC® chip used in this work. Authors S.P.M., M.D.K., M.M., and M.W.S. are employees of Nova Research Inc., 1900 Elkins St. Suite 230, Alexandria VA 22308 USA.

References

Andreotti, P.E., Ludwig, G.V., Peruski, A.H., Tuite, J.J., Morse, S.S., Peruski, J., L. F., 2003. BioTechniques 35, 850-859.

Baeumner, A.J., 2003. Analytical and Bioanalytical Chemistry 377, 434-445.

Bange, A., Halsall, H.B., Heineman, W.R., 2005. Biosensors and Bioelectronics 20, 2488-2503.

Baselt, D.R., Lee, G.U., Natesan, M., Metzger, S.W., Sheehan, P.E., Colton, R.J., 1998. Biosensors and Bioelectronics 13, 731-739.

Chang, K.-C., Hammer, D.A., 1996. Langmuir 12, 2271-2282.

Crowley, T.A., Pizziconi, V., 2005. Lab On A Chip 5, 922-929.

Decaro, N., Elia, G., Desario, C., Roperto, S., Martella, V., Campolo, M., Lorusso, A., Cavalli, A., Buonavoglia, C., 2006. Journal of Virological Methods 136, 65-70.

Edelstein, R.L., Tamanaha, C.R., Sheehan, P.E., Miller, M.M., Baselt, D.R., Whitman, L.J., Colton, R.J., 2000. Biosensors and Bioelectronics 14, 805-813.

Epstein, J.R., Biran, I., Walt, D.R., 2002. Analytica Chimica Acta 469, 3-36.

Erickson, D., Li, D.Q., 2004. Analytica Chimica Acta 507, 11-26.

Farre, M., Barcelo, D., 2003. Trac-Trends In Analytical Chemistry 22, 299-310.

Gao, X., Mathieu, H.J., Schawaller, M., 2004. Surface and Interface Analysis 36, 1507-1512.

Goldman, A.J., Cox, R.G., Brenner, H., 1967. Chemical Engineering Science 22, 653-660.

Graham, D.L., Ferreira, H.A., Freitas, P.P., 2004. Trends In Biotechnology 22, 455-462.

Hindson, B.J., Makarewicz, A.J., Setlur, U.S., Henderer, B.D., McBride, M.T., Dzenitis, J.M., 2005. Biosensors & Bioelectronics 20, 1925-1931.

Hoffmann, B., Depner, K., Schirrmeier, H., Beer, M., 2006. Journal of Virological Methods 136, 200-209.

Ivnitski, D., O'Neil, D.J., Gattuso, A., Schlicht, R., Calidonna, M., Fisher, R., 2003. BioTechniques 35, 862-869.

Kaur, J., Vikas Singh, K., Hirlekar Schmid, A., Varshney, G.C., Raman Suri, C., Raje, M., 2004. Biosensors and Bioelectronics 20, 284-293.

Lee, G.U., Chrisey, L.A., Colton, R.J., 1994. Science 266, 771-773.

Lee, G.U., Metzger, S., Natesan, M., Yanavich, C., Dufrene, Y.F., 2000. Analytical Biochemistry 287, 261-271.

Lee, T.M.H., Hsing, I.M., 2006. Analytica Chimica Acta 556, 26-37.

Lim, D.V., Simpson, J.M., Kearns, E.A., Kramer, M.F., 2005. Clinical Microbiology Reviews 18, 583-607.

Metzger, S.W., Natesan, M., Yanavich, C., Schneider, J., Lee, G.U., 1999. Journal of Vacuum Science and Technology A 17, 2623-2628.

Michalet, X., Kapanidis, A.N., Laurence, T., Pinaud, F., Doose, S., Pflughoefft, M., Weiss, S., 2003. Annual Review of Biophysics and Biomolecular Structure 32, 161-182.

Mulvaney, S.P., Mattoussi, H.M., Whitman, L.J., 2004. Biotechniques 36, 602-609.

Nam, J.-M., Stoeva, S.I., Mirkin, C.A., 2004. Journal of the American Chemical Society 126, 5932-5933.

Narang, U., Anderson, G.P., Ligler, F.S., Burans, J., 1997. Biosensors and Bioelectronics 12, 937-945.

Perrin, A., Duracher, S., Perret, M., Cleuziat, P., Mandrand, B., 2003. Analytical Biochemistry 322, 148-155.

Peruski, J., L. F., Peruski, A.H., 2003. BioTechniques 35, 840-846.

Rife, J.C., Miller, M.M., Sheehan, P.E., Tamanaha, C.R., Tondra, M., Whitman, L.J., 2003. Sensors and Actuators A-Physical 107, 209-218.

Rife, J.C., Whitman, L.J., 2004. Fluidic Force Discrimination. In: States, U. (Ed.), United States.

Saiki, R.K., Scharf, S., Faloona, F., Mullis, K.B., Horn, G.T., Erlich, H.A., Arnheim, N., 1985. Science 230, 1350-1354.

Sheehan, P.E., Edelstein, R.L., Tamanaha, C.R., Whitman, L.J., 2003. Biosensors and Bioelectronics 18, 1455-1459.

Sheehan, P.E., Whitman, L.J., 2005. Nano Letters 5, 803-807.

Stine, R., Cole, C.L., Ainslie, K.M., Mulvaney, S.P., Whitman, L.J., 2007. Langmuir, in press.

Stoeva, S.I., Lee, J.S., Smith, J.E., Rosen, S.T., Mirkin, C.A., 2006. Journal of The American Chemical Society 128, 8378-8379.

Tamanaha, C.R., Whitman, L.J., Colton, R.J., 2002. Journal of Micromechanics and Microengineering 12, 347-347.

Wang, S.X., Bae, S.Y., Li, G.X., Sun, S.H., White, R.L., Kemp, J.T., Webb, C.D., 2005. Journal of Magnetism and Magnetic Materials 293, 731-736.

Yi, C.Q., Li, C.W., Ji, S.L., Yang, M.S., 2006. Analytica Chimica Acta 560, 1-23.

Zheng, G., Patolsky, F., Cui, Y., Wang, W.U., Lieber, C.M., 2005. Nature Biotechnology 23, 1294-1301.

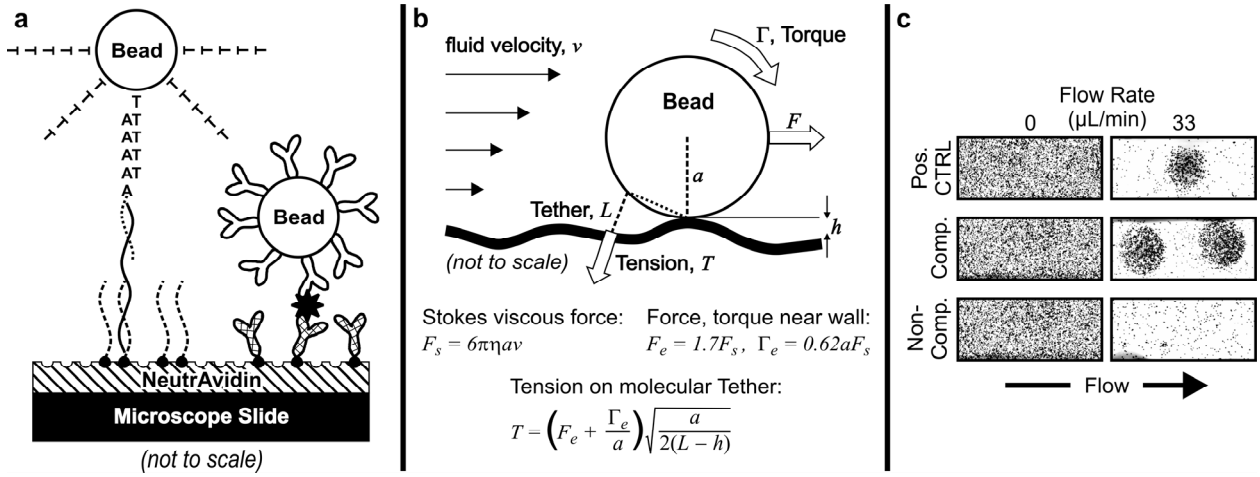

Fig. 1. Principles of fluidic force discrimination. (a) Illustration of the assay schemes for nucleic acid hybridization and immunological assays labeled with microbeads. (b) Free body diagram and mathematical model describing the forces on a microbead tethered to a surface in laminar flow[17]. F_s is the Stokes force on the bead, with v the fluid velocity at the bead center, η the viscosity, and a the bead radius. F_e and Γ_e are the exact hydrodynamic force and torque, respectively[20]. In the presence of surface roughness, h is the elevation of the bead-surface contact point relative to the tether-surface contact point. T is the tension force on a molecular tether of length L. (c) Optical micrographs demonstrating FFD applied to DNA detection. One positive control spot, two complementary, and two noncomplementary probe spots are shown before and after application of laminar flow forces. Each spot is 200 μm in diameter, with the 2.8 μm-diameter beads individually resolved.

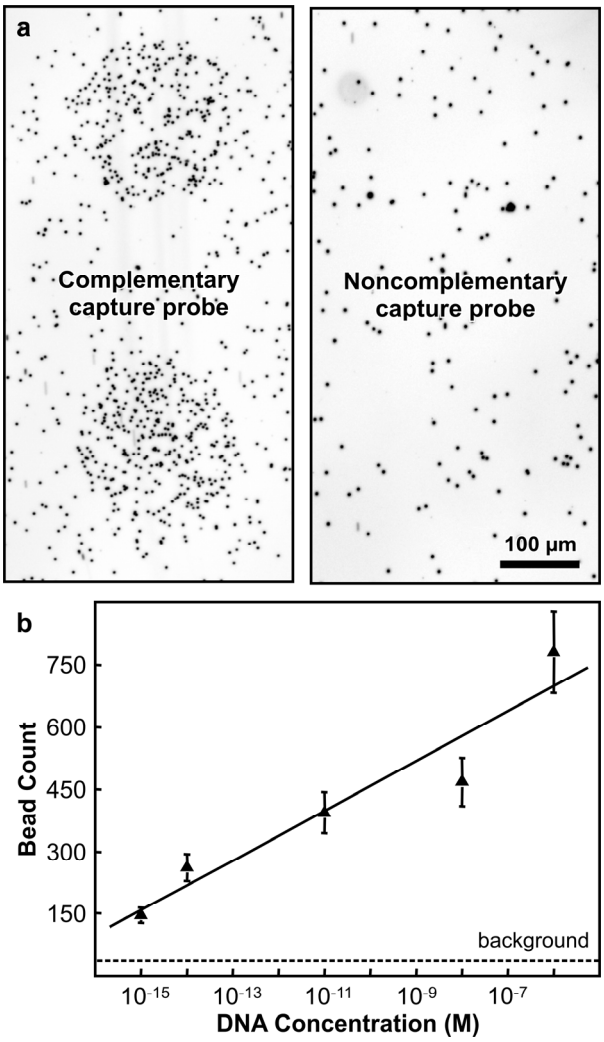

Fig. 2. Multiplexed DNA detection. (a) Multiplexed hybridization assay with 10 fM ssDNA target in buffer, showing micrographs of two complementary and two noncomplementary capture probe spots. (b) Dose-response curve based on bead labels counted within a 200 µm-diameter spot. The background line represents the average bead count for zero target concentration.

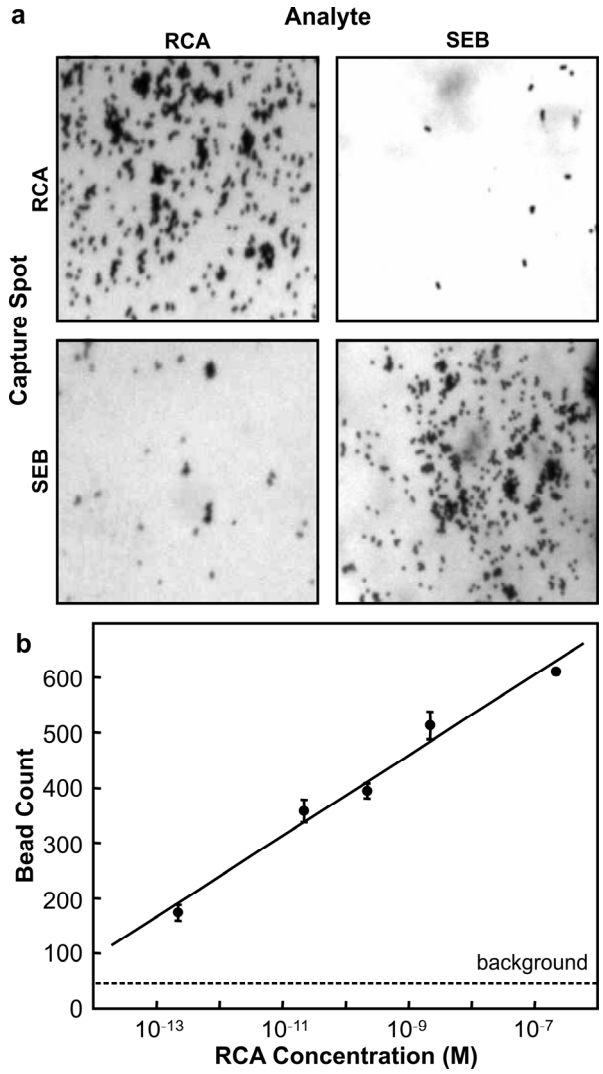

Fig. 3. Multiplexed protein toxin detection in buffer. (a) Multiplexed protein toxin immunoassays for RCA and SEB. Capture probe spots for each are shown with the detection of 218 pM (7ng/ml) RCA or 35 pM (1 ng/ml) SEB demonstrated. (b) Dose-response curve for RCA immunoassay based on bead labels counted within a 200 μm-diameter spot. The background line represents the average bead count on the SEB capture spot.

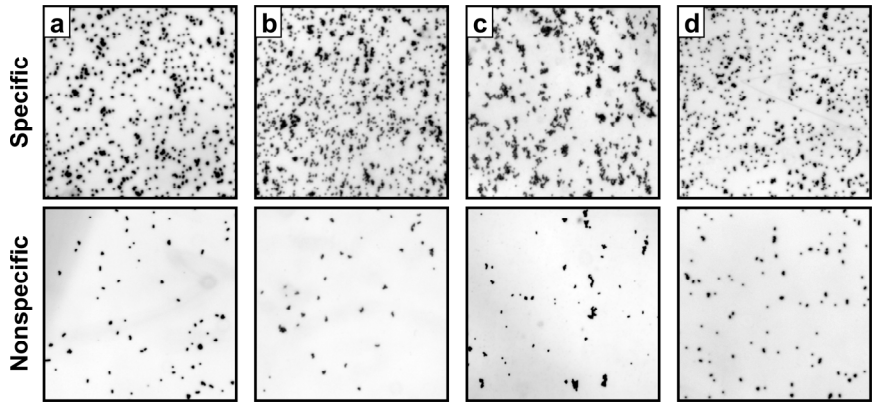

Fig. 4. Multiplexed Immunoassays in complex samples. Micrographs of capture probe microarray locations following multiplexed immunoassays for protein targets in various matrices (see METHODS for details). (a) 13 fM (2 pg/ml) IgG in plasma; (b) 280 fM (10 pg/ml) troponin I in serum; (c) 630 fM (20 pg/ml) ricin in whole milk; (d) IgG in whole blood diluted 10-fold in PBS (final concentration 13 fM or 2 pg/ml). The field of view of each micrograph is 300 μm × 300 μm (individual microbeads are visible). The negative controls ("Nonspecific") were spotted with antibodies against other targets.

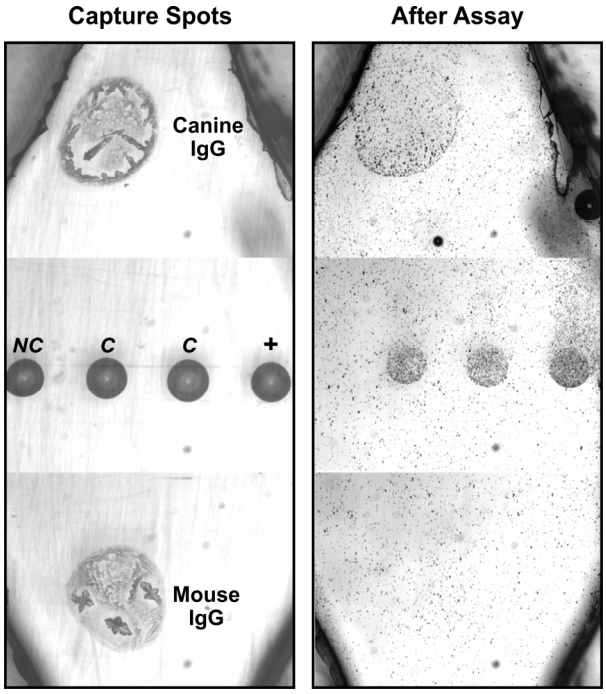

Fig. 5. Simultaneous DNA hybridization and protein immunoassay. Low magnification view of a substrate arrayed with two antibody capture probes and DNA capture probes for a positive control, two complementary (C), and a noncomplementary (*NC*) spot. The dried surface before the assay is shown on the left, indicating the location of the capture probes. The sample consisted of buffer spiked with 6.5 nM rabbit anti-canine IgG and 5 nM ssDNA (prehybridized with a label probe). The assay was performed with a mixture of sheep anti-rabbit and oligo$(dT)_{25}$ microbead labels, and demonstrates the potential for orthogonal assays in a single platform.

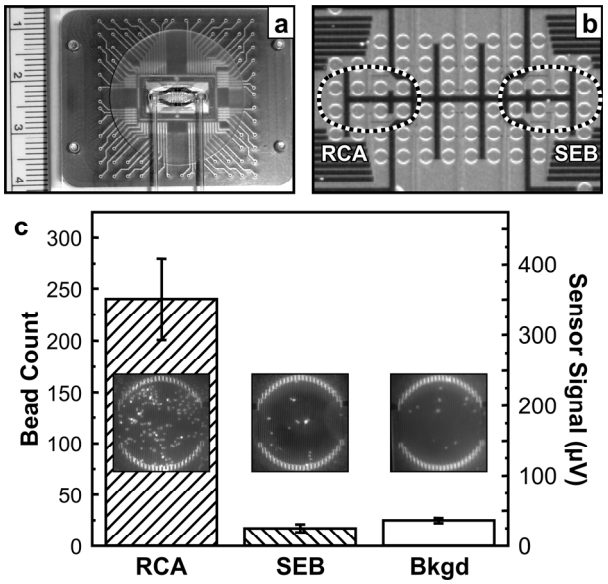

Fig. 6. Detection of 312 pM RCA in serum with the cBASS biosensor. (a) Photograph of the BARC® chip mounted in *cBASS* cartridge with tapered flow cell (ruler inset at left in cm). (b) Micrograph of a 64-sensor BARC® chip with multi-sensor capture zones for RCA and SEB as indicated. Each white circle is the outline of a 200 μm-diameter sensor (a single, serpentine GMR wire). (c) Graph depicting the average sensor response for the detection of 312 pM RCA in serum. The left axis shows the average bead count per sensor as determined by optical counting. The right axis shows the average voltage measured per sensor, which is linear in bead count up to ~1000 beads. Representative micrographs of individual sensors from each capture zone are inset.

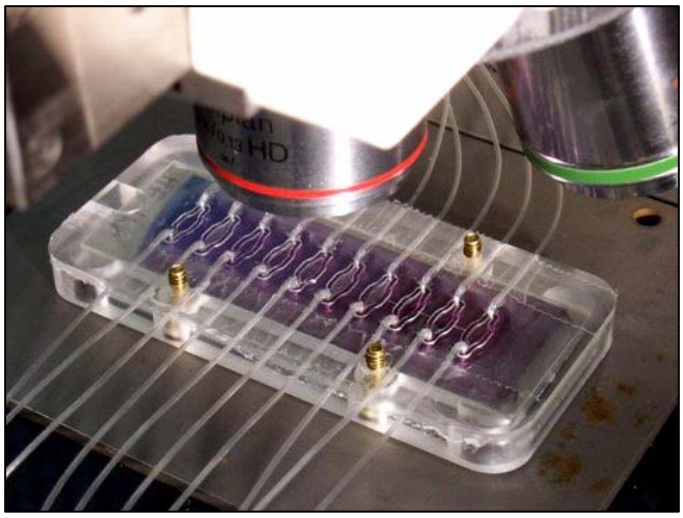

Supplemental Fig. 1. Assay fluidics. Photograph of the acrylic microfluidic apparatus in which the assays were performed, incorporating 10 individual flow cells mounted on a microscope slide and sealed with a PDMS gasket. Each flow cell had central dimensions of 2.8 mm long × 2.2 mm wide × 100 μm high, with tapered entrance and exits. The flow rates were controlled with a peristaltic pump. The apparatus was mounted on a standard upright microscope for optical bead counting.

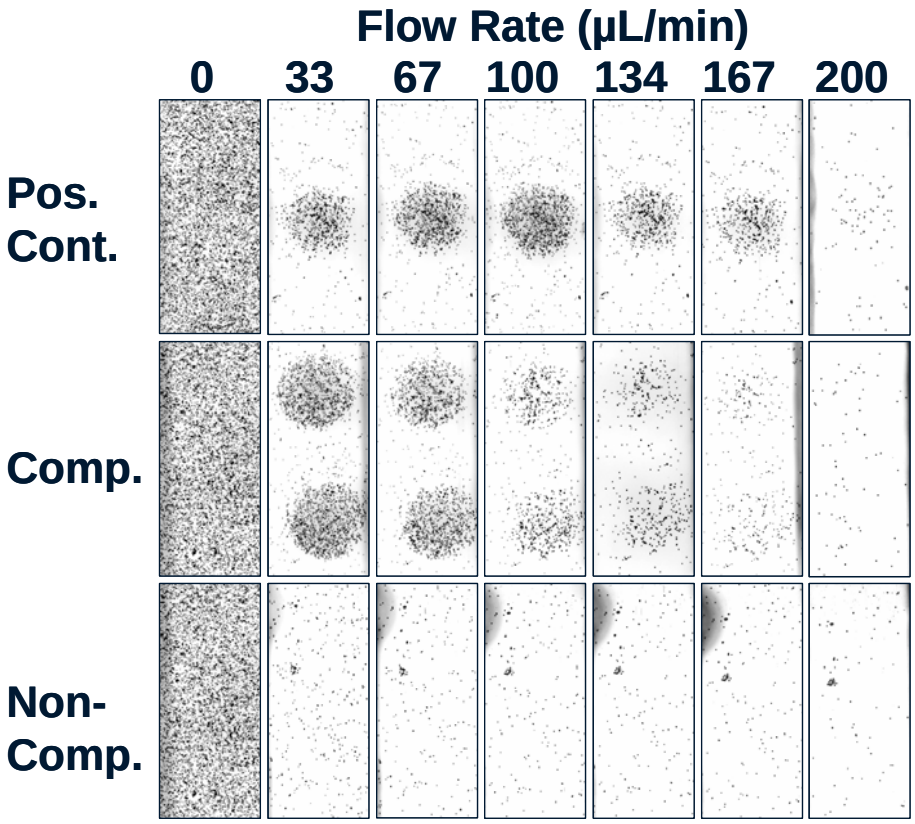

Supplemental Fig. 2. Flow rate depenedence of fluidic force discrimination. Optical micrographs showing bead removal vs. flow rate following DNA hybridization and microbead labeling. A positive control spot, two complementary spots, and two noncomplementary spots are shown at each flow rate (each 200 µm in diameter). The left column shows the surface after bead settling. Subsequent columns show beads remaining after applying a flow at the indicated rate for 2 min. At lower flow rates nonspecifically-bound beads are preferentially removed. At higher rates enough force is applied to remove beads attached through specific biomolecular interactions, rupturing the DNA duplexes.